

pubs.acs.org/JPCL Letter

Quantitative Study of the Energy Changes in Voltage-Controlled Spin Crossover Molecular Thin Films

Aaron Mosey, Ashley S. Dale, Guanhua Hao, Alpha N'Diaye, Peter A. Dowben, and Ruihua Cheng*



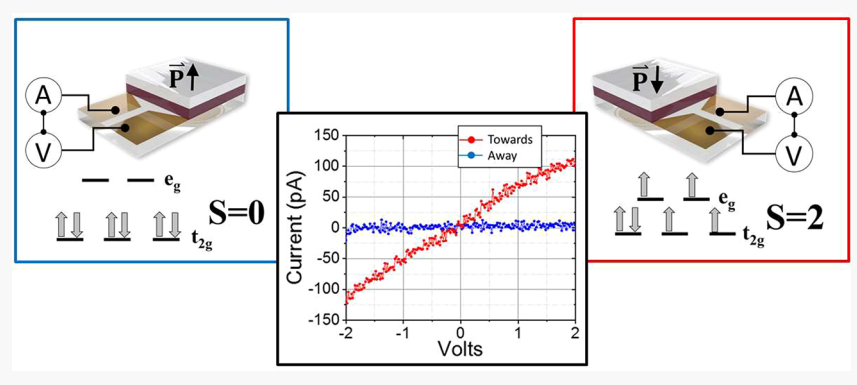
Cite This: J. Phys. Chem. Lett. 2020, 11, 8231–8237



ACCESS

Metrics & More

Article Recommendations



ABSTRACT: Voltage-controlled nonvolatile isothermal spin state switching of a $[Fe\{H_2B(pz)_2\}_2(bipy)]$ (pz = tris(pyrazol-1-1y)-borohydride, bipy = 2,2'-bipyridine) film, more than 40 to 50 molecular layers thick, is possible when it is adsorbed onto a molecular ferroelectric substrate. Accompanying this high-spin and low-spin state switching, at room temperature, we observe a remarkable change in conductance, thereby allowing not only nonvolatile voltage control of the spin state ("write") but also current sensing of the molecular spin state ("read"). Monte Carlo Ising model simulations of the high-spin state occupancy, extracted from X-ray absorption spectroscopy, indicate that the energy difference between the low-spin and high-spin state is modified by 110 meV. Transport measurements demonstrate that four terminal voltage-controlled devices can be realized using this system.

Voltage-controlled molecular multiferroics present an exciting new platform for the exploration of nonvolatile spin state switching, providing a basis for successful switchable nanoscale molecular devices. While electric field control of magnetism in oxide-based multiferroics is a well-established field, demonstrated molecular multiferroic phenomena have recently gained much attention. The molecular spin state may be addressed at the nanoscale suitched with high cyclability without degradation. Switching speed between the two spin states is potentially in the device-relevant GHz regime, while molecular-based systems are low-cost and can be produced using high-throughput processes such as stamping and printing. These desirable characteristics provide promising solutions for challenges faced by the nanoelectronics engineering community.

Spin crossover (SCO) transitions, in Fe(II) molecular complexes, may be induced by temperature, pressure, light, magnetic field, or electric field. The fundamental mechanism for SCO transition in Fe(II) coordination compounds resides in the ligand field theory, where the t_{2g} and e_g bands splitting affects low-spin (LS) S=0 and high-spin (HS) S=2 spin state occupancy in a reversable spin transition phenomenon. The locking and unlocking of the spin state in

[Fe{H₂B(pz)₂}₂(bipy)] molecules have been convincingly demonstrated in a number of studies.^{3,7,23–25} This nonvolatile locking of spin state has been achieved by adsorption of SCO molecules onto dielectric or polarized surface,^{3,7,23,25} and the spin state, in some examples, can be controlled with an external magnetic field³ or electric field (i.e., an applied voltage in the latter case).^{7,23} This switching from LS to HS, or the reverse, is accompanied by a profound change in conductivity.⁷ The ability to sense spin state change by current measurement in the picoampere regime, and the voltage control of the spin state via polarization of the ferroelectric substrate, are boons for engineered applications and make the study of multiferroic behaviors of this system accessible. When the molecular environment includes adsorption onto a polarized substrate, the exact nature of the interactions in play, affecting spin state

Received: July 20, 2020 Accepted: September 2, 2020 Published: September 3, 2020





population shifts, is an open question, ²⁶ especially as cooperative and entropic effects are known to have a role in the spin state bistability. ^{15,20,22,27–31}

It has been established that a polar interface, such as a ferroelectric substrate^{23,25,32} or the addition of dipolar molecules, 33 may perturb the activation energies for the lowspin to high-spin state transition. We present, here, a quantitative study of the energy scale and the accompanying conductance change associated with spin state switching in a layered molecular heterostructure with a thin film of the coordination compound $[Fe\{H_2B(pz)_2\}_2(bipy)]$, where py = tris(pyrazole-1-y1)-borohydride and bipy = 2,2'-bipyridine), adsorbed onto a thin film of ferroelectric polyvinylidene fluoride hexafluoropropylene (PVDF-HFP). The polarization of the ferroelectric was isothermally switched to opposite directions at 298 K through an external applied voltage, prompting the partial spin state change of the central Fe(II) ion from HS state S = 2 to LS state S = 0. In this study, a $[Fe\{H_2B(pz)_2\}_2(bipy)]$ film thickness of more than 40 to 50 molecular layers (65 nm thick) was chosen so that the influence of the ferroelectric substrate was diminished but not completely ineffectual. Here both temperature and voltage have an influence on the spin state, unlike for [Fe{H₂B- $(pz)_2$ ₂(bipy)] thin films of less than 20 to 25 molecular layers, where the ferroelectric interface polarization appears to dominate, suppressing the influence of temperature.

Three distinct samples were fabricated. Device 1, a multilayered heterostructure illustrated in Figure 1, was used

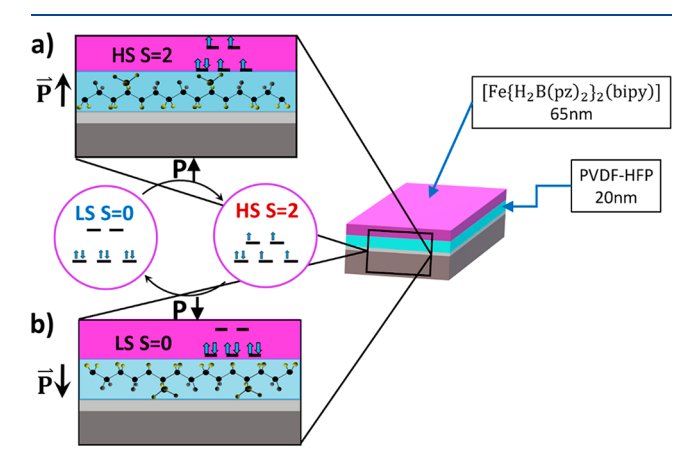


Figure 1. Configuration for multilayered thin-film samples (device 1) used to characterize the spin state of the $[Fe\{H_2B(pz)_2\}_2(bipy)]$ (red) when coupled to the polarization of a ferroelectric PVDF-HFP layer (blue). From bottom to top, the structure is silicon substrate, bottom electrode of 80 nm titanium, 20 nm PVDF-HFP, and 65 nm $[Fe\{H_2B(pz)_2\}_2(bipy)]$.

for the X-ray absorption spectroscopy (XAS) experiments. Devices 2 and 3, illustrated in Figures 4 and 5, respectively, are thin-film samples that incorporate interdigitated electrodes for transport measurements. Shown in Figure 4b, the electrodes for the transport studies are based on an array of interdigitated Au electrodes 250 nm thick and 10 μ m wide with an intradigit spacing of 5 μ m.

Device 1 was constructed as follows: A bottom electrode consisting of an 80 nm Ti thin film was deposited on a silicon substrate by DC magnetron sputtering in high vacuum, followed by a 20 nm layer of PVDF-HFP produced by Langmuir—Blodgett (LB) deposition, then a 65 nm layer of

[Fe{ $H_2B(pz)_2$ }_2(bipy)] was grown on top of the ferroelectric PVDF-HFP via thermal evaporation in high vacuum. The PVDF-HFP thin films were fabricated using layer-by-layer LB deposition following established methods, 34,35 while thermal deposition of the [Fe{ $H_2B(pz)_2$ }_2(bipy)] was performed following the same procedure as our previous experiments 3,7,23–25 and has been adopted by others. 36 Poling of the ferroelectric layer was achieved by placing a removeable electrode which is a copper plate mounted on a micrometer stage on top of the sample and applying a voltage (10 V) across the heterostructure. The applied voltage created an electric field of ~120 MV/m perpendicular to the plane of the structure, which is above the coercive field (~100 MV/m) required to create a single, polarized domain for PVDF-HFP.

X-ray absorption spectroscopy, in total electron yield (TEY) mode at the Fe L_3 edge, was used to probe the unoccupied Fe weighted e_g and t_{2g} molecular orbitals of $[Fe\{H_2B-(pz)_2\}_2(bipy)]$, as a function of the ferroelectric polarization of the adjacent PVDF-HFP thin film. This provided a clear picture that the spin state of the $[Fe\{H_2B(pz)_2\}_2(bipy)]$ thin film depends upon the polarization direction of the PVDF-HFP layer. Measurements were done at the Advanced Light Source at Lawrence Berkeley National Laboratory on bending magnet beamline 6.3.1, with TEY mode configured using circularly polarized, positive helicity photons with a photon flux of 10^{11} photons/sec/0.1%BW. These parameters are the same as used in prior studies.^{7,23,25,27} The intensity of the X-ray beam was tuned in order to limit photoactivation of the molecule yet maintain an acceptable TEY signal.

In-plane conductance measurements were taken on devices 2 and 3. Device 2, shown in Figure 4c, was fabricated to measure the conductance as a function of temperature only and consists of 65 nm of [Fe{H₂B(pz)₂}₂(bipy)] deposited directly on the interdigitated electrodes, mentioned above. Device 3 was used to characterize the spin state dependent conductance attributable to changes in the ferroelectric polarization, either up or down perpendicular to the plane (i.e., along the normal), and was prepared as follows: a 65 nm $[Fe\{H_2B(pz)_2\}_2(bipy)]$ thin film was grown directly on the interdigitated electrode array; 20 nm of ferroelectric PVDF-HFP was then deposited upon this layer, and a top electrode of 80 nm Au was grown by thermal evaporation under high vacuum to avoid damaging the organic layers. The heterostructure was polarized by applying a voltage around 10 V between the bottom interdigitated electrodes and the top Au electrode. Conductance measurements were done using a two-probe technique with an applied voltage source and current readout by a pico-ammeter.

Using XAS, we have confirmed the prior observation 7,23 that when the ferroelectric PVDF-HFP is polarized up (schematically shown in Figure 1a), the $[Fe\{H_2B(pz)_2\}_2(bipy)]$ prefers the HS state with S=2, and when the ferroelectric PVDF-HFP is polarized down (schematically shown in Figure 1b), the LS state with S=0 is favored. Yet, we find that for $[Fe\{H_2B(pz)_2\}_2(bipy)]$ films 65 nm thick, the spin state occupancy is not only dependent upon the direction of ferroelectric polarization but also is temperature-dependent. The switching of HS to LS states at room temperature, through a voltage control, is clearly evident in the XAS measurements, as shown in Figure 2. In the absence of external electric stimuli, $[Fe\{H_2B(pz)_2\}_2(bipy)]$ is naturally in the HS state at 298 K, and the typical reported $T_{1/2}$ from the HS state to LS state is around 167 K.^{27,40} Figure 2a shows the

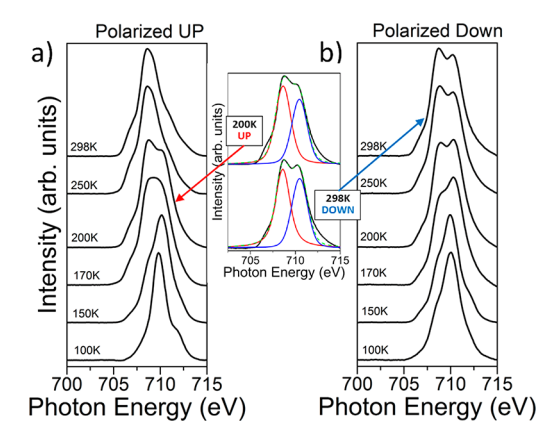


Figure 2. X-ray absorption spectra showing the changing intensities of the e_g and t_{2g} features for $[Fe\{H_2B(pz)_2\}_2(bipy)]$, as a function of temperature and substrate ferroelectric polarization. In panel a, the PVDF-HFP substrate is polarized "up" or toward the SCO layer. In panel b, the PVDF-HFP substrate is polarized "down" or away from the SCO film as unoccupied states of the e_g orbital above the transition temperature are observed, indicating that the sample can be locked into the low-spin S=0 state above the transition temperature of 167 K. Each spectrum is deconvoluted into HS dominant (red curve) and LS dominant (blue curve) peaks, shown in the inset between panels a and b.

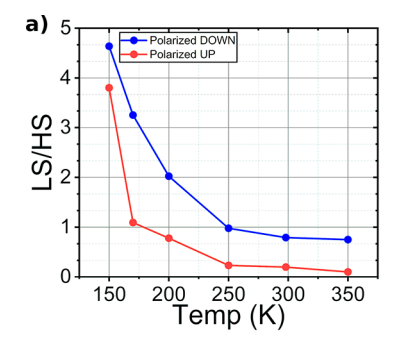
temperature-dependent XAS data for $[Fe\{H_2B(pz)_2\}_2(bipy)]$ thin films deposited on a ferroelectric PVDF-HFP substrate when PVDF-HFP is polarized "up", i.e., toward the SCO layer, as schematically illustrated in Figure 1a, while Figure 2b shows the data when PVDF-HFP is polarized "down" or away from the SCO layer, as schematically illustrated in Figure 1b. When $[Fe\{H_2B(pz)_2\}_2(bipy)]$ is in the LS state, the 3d electrons occupy the t_{2g} in pairs, leaving the e_g molecular orbital empty. This unoccupied e_g molecular orbital is observable in the $2p_{3/2}$ (Fe L₃) XAS spectra as a major peak, at a photon energy of about 710 eV. In the high-spin state, the e_{σ} is partially populated with the t_{2g} orbitals subsequently partly depopulated. This leads to a signature of the t_{2g} in the XAS spectra at the Fe L₃ $(2p_{3/2})$ edge with features appearing at photon energies of 704 and 708 eV, while the feature at 710 eV, characteristic of the e_{σ} molecular orbital, decreases.

There are significant differences in the XAS spectra for $[Fe\{H_2B(pz)_2\}_2(bipy)]$ when the PVDF-HFP substrate is polarized "down" versus polarized "up". Figure 2b shows the temperature-dependent XAS data for $[Fe\{H_2B(pz)_2\}_2(bipy)]$

deposited on a ferroelectric PVDF-HFP substrate when PVDF-HFP is polarized "down" or away from the SCO layer, as illustrated in Figure 1b, and the signature of the e_{σ} unoccupied molecular orbital (at a photon energy of 710 eV) remains strong at all temperatures. This indicates that the sample can be locked mostly (but imperfectly) into the LS S = 0 state above the powder transition temperature of 167 K.4,27,40 As shown in Figure 2a, when PVDF-HFP is polarized "up" or toward the $[Fe\{H_2B(pz)_2\}_2(bipy)]$ thin-film layer, as sketched in Figure 1a, the signature of the e_g orbital dominates the XAS spectra only below 150 K. When the sample temperature is raised beyond 150 K, when the ferroelectric substrate is polarized "up" or toward the $[Fe\{H_2B(pz)_2\}_2(bipy)]$ thin film, a distinct peak is evident in the region of the photon energy of 708 eV, accompanied by a small shoulder at 704 eV, characteristic of the t_{2g} unoccupied molecular orbitals, as noted above, and a signature of the S = 2 HS state.

Considering the evolution of density of states for t_{2g} and e_g orbitals as a function of changing temperature, in the different electric field orientation as produced by the polarized ferroelectric layer, the energetics involved in the electric field-induced transition between the HS and LS states may be examined. As shown in the inset between panels a and b in Figure 2, the resolved peaks of HS and LS states for all the spectra taken at different temperatures with two opposite polarization directions indicate that comparable LS to HS state ratios (γ_{LS}) exist at 200 K for the ferroelectric substrate polarized "up" while a similar ratio is observed at 298 K for the ferroelectric substrate polarized "down". The spin state occupancy, as a function of temperature and ferroelectric substrate polarization, is summarized in Figure 3. The LS-to-HS state ratio data in Figure 3a and the HS state occupancy in Figure 3b consistently show that the choice of substrate polarization creates a temperature difference between the relative HS-to-LS state occupancies. Considering the LS-to-HS state ratio $\gamma_{LS} = 1$, we can clearly observe that the SCO transition takes place in the temperature region of 170 K for "up" and 250 K for "down" or a temperature difference of around 80 K in assessing the effect of the substrate polarization (toward or away from the SCO molecular layer, i.e., polarized up or down) on the high-spin state occupancy.

The phase transition between HS and LS states of SCO molecules can be simulated by an Ising-like model, where the two discrete values correspond to the HS and LS states, respectively.³⁸ In order to understand the mechanism of how



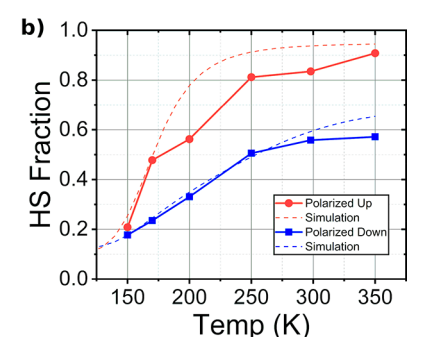


Figure 3. Comparable ratios of low-spin (LS) state to high-spin (HS) state for different temperatures and polarization, as measured by XAS on device 1. Figure 3a is a plot of γ_{LS} (LS/HS ratio) as a function of temperature for two different polarized directions, as derived from the XAS spectra; the red data curve is for the ferroelectric PVDF-HFP polarized up, and the blue data curve is for PVDF-HFP polarized down. HS fraction as a function of temperature is plotted in panel b, with the modified Monte Carlo Ising model simulation superimposed.

the electric polarization affects the transition temperature in the molecular $[Fe\{H_2B(pz)_2\}_2(bipy)]/PVDF$ -HFP bilayer system, we use a two-dimensional Monte Carlo Ising model^{39,40} simulation to generate the theoretical data shown in Figure 3b. The typical Hamiltonian expression for a SCO transition is

$$H = -J \sum_{(i,j)} S(i,j)S(i \pm 1, j \pm 1) + \left(\frac{\Delta}{2} - \frac{k_{\rm B}T}{2} \ln g\right) \sum_{(i,j)} S(i,j)$$

where I is the interaction between molecules, the HS and LS take +1 and -1 for spin operator S(i, j), Δ is the energy difference between HS and LS states of isolated molecules, and ln g is the ratio of HS degeneracy to LS degeneracy. Simulation data, shown as the dashed lines in Figure 3b, indicates that the energy difference Δ between HS and LS states is approximately 88 meV when the ferroelectric substrate is polarized up while parameter Δ increases to approximately 198 meV when the polarization is switched to the opposite direction. The energy difference in the Δ , between HS and LS states, as a result of the different substrate ferroelectric polarizations, is approximately 110 meV. This ferroelectric substrate polarizationdependent energy difference Δ is indicative of significant changes within the $[Fe\{H_2B(pz)_2\}_2(bipy)]$ thin film that are clearly substrate dependent. While the substrate has been seen previously to affect the spin state bistability, 7,23-25,27 here the results show that the polarization direction, of the ferroelectric substrate, plays an important role. Considering that the electrical dipole moment in $[Fe\{H_2B(pz)_2\}_2(bipy)]$ is 4.7 D for the LS state, 25 we estimate the electrical field generated from the polarized ferroelectric PVDF-HFP is at least 4.9×10^9 V/m, at the interface, when the field is parallel with the $[Fe\{H_2B(pz)_2\}_2(bipy)]$ dipole moment. In general, these two vectors are unlikely to be perfectly aligned in parallel, implying that the actual electric field due to the polarization of the PVDF-HFP may be much higher than this estimated value. This result is in agreement with our previous study for PVDF thin films.³⁸ The crystallization of the PVDF-HFP layer is crucial to observing this polarization effect, where lack of crystallization will result in the random distribution of dipole moments and diminish the net interface dipole. Improved order and crystallization of β -phase PVDF-HFP thin films⁴ allows for more uniform polarization and thus higher electric field. This does not exclude the possibility that interactions at the interface between the PVDF-HFP layer and the [Fe{H₂B- $(pz)_2$ ₂(bipy)] propagate through the $[Fe{H_2B(pz)_2}_2(bipy)]$ thin film and this interaction also depends on a high degree of crystallinity. The electric field is similar in magnitude for a ferroelectric polarization toward or away from the SCO $[Fe\{H_2B(pz)_2\}_2(bipy)]$ layer, but the interface termination changes from largely hydrogen termination at the interface, with the PVDF-HFP layer poled toward the SCO [Fe{H₂B-(pz)₂}₂(bipy)] molecular layer, to a fluorine termination for a polarization away from the SCO $[Fe\{H_2B(pz)_2\}_2(bipy)]$ molecular layer. When initially adsorbed onto the substrate, SCO may have a preferential orientation with respect to the PVDF-HFP, and it is sterically hindered from molecular rotation when the ferroelectric polarization is then reversed. This has some effect, because the intrinsic [Fe{H₂B-(pz)₂{2(bipy)] dipole is then perturbed differently as the interface electric field changes sign. However, presently there is no direct evidence as to the mechanism for the ferroelectric

substrate polarization perturbation of the $[Fe\{H_2B-(pz)_2\}_2(bipy)]$ spin states.

These XAS data, supported by the 2D Ising model simulations, suggest a profound interaction between the $[Fe\{H_2B(pz)_2\}_2(bipy)]$ spin crossover layer and the ferroelectric at the interface. The lack of a more complete adoption of the high-spin state at 200 K, when PVDF-HFP is polarized "up" (Figure 2a), and the signatures of partial occupancy of the low-spin state throughout the measured temperature range, when PVDF-HFP is polarized "down" (Figure 2b), is the result of a thicker $[Fe\{H_2B(pz)_2\}_2(bipy)]$ spin crossover film. In some prior studies, where the $[Fe\{H_2B(pz)_2\}_2(bipy)]$ film was only a few molecular layers²³ (less than 12 nm) of $[Fe\{H_2B(pz)_2\}_2(bipy)]$, the HS and LS states were more strongly favored over a broad range of temperatures when the ferroelectric substrate was polarized "up" or "down", respectively. Cooperative and surface effects are known and could also influence the measured spin state occupancy.²

Conductance changes, associated with the different spin state change, are well-documented in SCO materials $^{12,22,43-54}$ and can be used to induce conductance changes in an adjacent graphene layer. Yet nonvolatile changes in the conductivity of SCO molecules, associated with a static polarization of an adjacent ferroelectric layer, have just recently been characterized. The conventional approach to induce the SCO transition from HS to LS is through temperature control, and this holds for the SCO $[Fe\{H_2B(pz)_2\}_2(bipy)]$ as well. As shown in Figure 4a, the I-V curves for temperatures 298 and

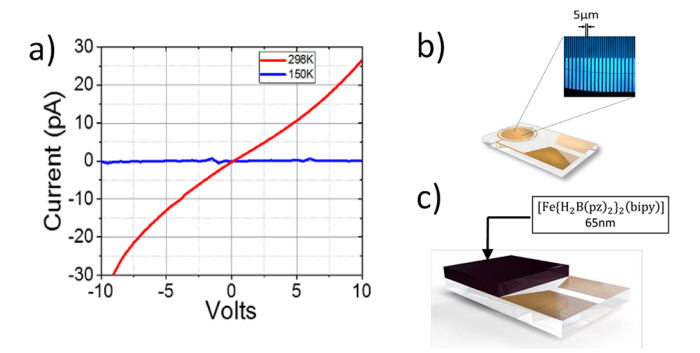


Figure 4. Differences in conductance for $[Fe\{H_2B(pz)_2\}_2(bipy)]$ thin films for the high-spin (HS) dominated state versus the low-spin (LS) dominated state. Panel a shows the conductance measured across device 2 at room temperature (298 K) and below $T_{1/2}$, the transition temperature (150 K). Interdigitated electrodes with a spacing of 5 μ m were used as the basis for all transport measurement, as shown in panel b. As shown in panel c, device 2 consists of a $[Fe\{H_2B-(pz)_2\}_2(bipy)]$ thin film deposited directly on interdigitated electrodes.

150 K are plotted. Data for the 298 K measurement clearly show a nonlinear response, well above the spin transition $T_{1/2}$, at 167 K. Below the spin transition $T_{1/2}$, at 150 K, a dramatic decrease in conductance, by about 2 orders of magnitude, is observed, which is consistent with the larger highest occupied molecular orbital (HOMO) to lowest unoccupied molecular orbital (LUMO) gap $[Fe\{H_2B(pz)_2\}_2(bipy)]^{23}$ and the resulting low conductance in LS states noted elsewhere.

Here the temperature-dependent conductance of SCO $[Fe\{H_2B(pz)_2\}_2(bipy)]$ thin film is mediated by the ferroelectric substrate polarization as well as temperature; Figure 5 shows the polarization-dependent conductance data measured

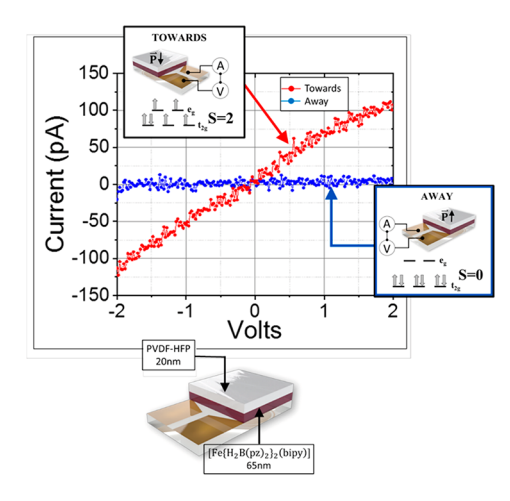


Figure 5. The changes in conductance observed with different ferroelectric polarization directions. Transport measurements were taken across a device with the ferroelectric layer adjacent to the SCO layer. Polarizing the ferroelectric toward the $[Fe\{H_2B(pz)_2\}_2(bipy)]$ layer results in HS S=2, and a larger conductance. Polarization of the ferroelectric away from the $[Fe\{H_2B(pz)_2\}_2(bipy)]$ layer gives the low spin S=0 state and lower conductance by 2 orders of magnitude. Device 3 is schematically illustrated.

at 298 K for the multilayer system of the $[Fe\{H_2B-(pz)_2\}_2(bipy)]/PVDF-HFP$ thin-film heterostructure, as described in the configuration of device 3. When the polarization of the ferroelectric layer is polarized toward the $[Fe\{H_2B-(pz)_2\}_2(bipy)]$ layer, the HS state is dominant, and a higher conductance is observed. The conductance of the $[Fe\{H_2B-(pz)_2\}_2(bipy)]$ thin film is clearly mediated by the polarization of the ferroelectric PVDF-HFP substrate, which in turn can be controlled by a gate voltage and is nonvolatile, creating a straightforward route toward a three terminal molecular device. ¹

These studies clearly demonstrate that a bistable isothermal switching of the spin state and conductance in [Fe{H₂B- $(pz)_2$ ₂(bipy)] thin films may be controlled by the application of an external voltage when adsorbed onto a ferroelectric substrate. Insight into the switching mechanism is gained through XAS and theoretical modeling, further unveiling the mechanism of switching. Broadening of the energy gap between the HS and LS states, as characterized by XAS and examined with theoretical modeling, gives an energy change for this process of about 110 meV. Moreover, the bistable spin transition is accompanied by a measurable change in transport properties around 2 orders of magnitude between the HS and LS states on devices where the SCO is triggered by an applied external voltage. This nonvolatile voltage controlled switching of the molecular spin state supplies an intriguing, feasible platform for the design of gated voltage-controlled molecular spintronic devices.

AUTHOR INFORMATION

Corresponding Author

Ruihua Cheng — Department of Physics, Indiana University—Purdue University Indianapolis, Indianapolis, Indiana 46202, United States; oorcid.org/0000-0003-1579-8097; Email: rucheng@iupui.edu

Authors

Aaron Mosey — Department of Physics, Indiana University—Purdue University Indianapolis, Indianapolis, Indiana 46202, United States; o orcid.org/0000-0003-1513-3968

Ashley S. Dale — Department of Physics, Indiana University—Purdue University Indianapolis, Indianapolis, Indiana 46202, United States

Guanhua Hao — Department of Physics and Astronomy, University of Nebraska Lincoln, Lincoln, Nebraska 68588, United States; Advanced Light Source, Lawrence Berkeley National Laboratory, Berkeley, California 94720, United States

Alpha N'Diaye – Advanced Light Source, Lawrence Berkeley National Laboratory, Berkeley, California 94720, United States

Peter A. Dowben – Department of Physics and Astronomy, University of Nebraska Lincoln, Lincoln, Nebraska 68588, United States; Ocid.org/0000-0002-2198-4710

Complete contact information is available at: https://pubs.acs.org/10.1021/acs.jpclett.0c02209

Notes

The authors declare no competing financial interest.

ACKNOWLEDGMENTS

This research was supported by the National Science Foundation through NSF-Chem 1565692 and NSF-DMR 2003057 [A.M., A.S.D., G.H., R.C., and P.A.D.]. Use of the Advanced Light Source, Lawrence Berkeley National Laboratory, was supported by the U.S. Department of Energy (DOE) under contract no. DE-AC02-05CH11231. The authors acknowledge the artistic contributions to Figures 4 and 5 by Sara Dale.

REFERENCES

- (1) Hao, G.; Cheng, R.; Dowben, P. A. The Emergence of the Local Moment Molecular Spin Transistor. *J. Phys.: Condens. Matter* **2020**, 32 (23), 234002.
- (2) Vaz, C. A. F. Electric Field Control of Magnetism in Multiferroic Heterostructures. *J. Phys.: Condens. Matter* **2012**, 24 (33), 333201.
- (3) Zhang, X.; N'Diaye, A. T.; Jiang, X.; Zhang, X.; Yin, Y.; Chen, X.; Hong, X.; Xu, X.; Dowben, P. A. Indications of Magnetic Coupling Effects in Spin Cross-over Molecular Thin Films. *Chem. Commun.* **2018**, *54* (8), 944–947.
- (4) Zapf, V. S.; Sengupta, P.; Batista, C. D.; Nasreen, F.; Wolff-Fabris, F.; Paduan-Filho, A. Magnetoelectric Effects in an Organometallic Quantum Magnet. *Phys. Rev. B: Condens. Matter Mater. Phys.* **2011**, 83 (14), 22–25.
- (5) Zapf, V. S.; Kenzelmann, M.; Wolff-Fabris, F.; Balakirev, F.; Chen, Y. Magnetically Induced Electric Polarization in an Organometallic Magnet. *Phys. Rev. B: Condens. Matter Mater. Phys.* **2010**, 82 (6), 1–4.
- (6) Chikara, S.; Gu, J.; Zhang, X.-G. G.; Cheng, H.-P. P.; Smythe, N.; Singleton, J.; Scott, B.; Krenkel, E.; Eckert, J.; Zapf, V. S. Magnetoelectric Behavior via a Spin State Transition. *Nat. Commun.* **2019**, *10* (1), 4043.
- (7) Hao, G.; Mosey, A.; Jiang, X.; Yost, A. J. J.; Sapkota, K. R. R.; Wang, G. T. T.; Zhang, X.; Zhang, J.; N'Diaye, A. T. T.; Cheng, R.; Xu, X.; Dowben, P. A. A. Nonvolatile Voltage Controlled Molecular Spin State. *Appl. Phys. Lett.* **2019**, *114* (3), 032901.
- (8) Larionova, J.; Salmon, L.; Guari, Y.; Tokarev, A.; Molvinger, K.; Molnár, G.; Bousseksou, A. Towards the Ultimate Size Limit of the Memory Effect in Spin-Crossover Solids. *Angew. Chem., Int. Ed.* **2008**, 47 (43), 8236–8240.
- (9) Shepherd, H. J.; Molnár, G.; Nicolazzi, W.; Salmon, L.; Bousseksou, A. Spin Crossover at the Nanometre Scale. *Eur. J. Inorg. Chem.* **2013**, 2013, 653–661.
- (10) Piedrahita-Bello, M.; Martin, B.; Salmon, L.; Molnár, G.; Demont, P.; Bousseksou, A. Mechano-Electric Coupling in P(VDF-

- TrFE)/Spin Crossover Composites. J. Mater. Chem. C 2020, 8 (18), 6042-6051.
- (11) Usmani, S.; Mikolasek, M.; Gillet, A.; Sanchez Costa, J.; Rigoulet, M.; Chaudret, B.; Bousseksou, A.; Lassalle-Kaiser, B.; Demont, P.; Molnár, G.; Salmon, L.; Carrey, J.; Tricard, S. Spin Crossover in Fe(Triazole)-Pt Nanoparticle Self-Assembly Structured at the Sub-5 Nm Scale. *Nanoscale* **2020**, *12* (15), 8180–8187.
- (12) Lefter, C.; Rat, S.; Costa, J. S.; Manrique-Juárez, M. D.; Quintero, C. M.; Salmon, L.; Séguy, I.; Leichle, T.; Nicu, L.; Demont, P.; Rotaru, A.; Molnár, G.; Bousseksou, A. Current Switching Coupled to Molecular Spin-States in Large-Area Junctions. *Adv. Mater.* **2016**, 28 (34), 7508–7514.
- (13) Senthil Kumar, K.; Ruben, M. Emerging Trends in Spin Crossover (SCO) Based Functional Materials and Devices. *Coord. Chem. Rev.* **2017**, 346, 176–205.
- (14) Cavallini, M. Status and Perspectives in Thin Films and Patterning of Spin Crossover Compounds. *Phys. Chem. Chem. Phys.* **2012**, *14* (34), 11867–11876.
- (15) Mallah, T.; Cavallini, M. Surfaces, Thin Films and Patterning of Spin Crossover Compounds. C. R. Chim. 2018, 21 (12), 1270–1286.
- (16) Claeys, C. Trends and Challenges in Micro- and Nanoelectronics for the next Decade. In *Proceedings of the 19th International Conference Mixed Design of Integrated Circuits and Systems MIXDES* 2012; pp 37–42.
- (17) Wang, K. L. Issues of Nanoelectronics: A Possible Roadmap. J. Nanosci. Nanotechnol. 2002, 2 (3), 235–266.
- (18) Tsu, R. Challenges in Nanoelectronics. *Nanotechnology* **2001**, 12 (4), 625–628.
- (19) National Nanotechnology Initiative Signature Initiative: Nanoelectronics for 2020 and Beyond; 2010; pp 1–6.
- (20) Gütlich, P.; Garcia, Y.; Goodwin, H. A. Spin Crossover Phenomena in Fe(II) Complexes. *Chem. Soc. Rev.* **2000**, 29 (6), 419–427.
- (21) Lefter, C.; Tan, R.; Dugay, J.; Tricard, S.; Molnár, G.; Salmon, L.; Carrey, J.; Nicolazzi, W.; Rotaru, A.; Bousseksou, A. Unidirectional Electric Field-Induced Spin-State Switching in Spin Crossover Based Microelectronic Devices. *Chem. Phys. Lett.* **2016**, *644*, 138–141.
- (22) Prins, F.; Monrabal-Capilla, M.; Osorio, E. A.; Coronado, E.; van der Zant, H. S. J. Room-Temperature Electrical Addressing of a Bistable Spin-Crossover Molecular System. *Adv. Mater.* **2011**, 23 (13), 1545–1549.
- (23) Zhang, X.; Palamarciuc, T.; Létard, J.-F.; Rosa, P.; Lozada, E. V.; Torres, F.; Rosa, L. G.; Doudin, B.; Dowben, P. A. The Spin State of a Molecular Adsorbate Driven by the Ferroelectric Substrate Polarization. *Chem. Commun.* **2014**, *50* (18), 2255.
- (24) Beniwal, S.; Zhang, X.; Mu, S.; Naim, A.; Rosa, P.; Chastanet, G.; Létard, J.-F.; Liu, J.; Sterbinsky, G. E.; Arena, D. A.; Dowben, P. A.; Enders, A. Surface-Induced Spin State Locking of the [Fe(H 2 B(Pz) 2) 2 (Bipy)] Spin Crossover Complex. *J. Phys.: Condens. Matter* **2016**, 28 (20), 206002.
- (25) Zhang, X.; Costa, P. S.; Hooper, J.; Miller, D. P.; N'Diaye, A. T.; Beniwal, S.; Jiang, X.; Yin, Y.; Rosa, P.; Routaboul, L.; Gonidec, M.; Poggini, L.; Braunstein, P.; Doudin, B.; Xu, X.; Enders, A.; Zurek, E.; Dowben, P. A. Locking and Unlocking the Molecular Spin Crossover Transition. *Adv. Mater.* **2017**, 29 (39), 1702257.
- (26) Cinchetti, M.; Dediu, V. A.; Hueso, L. E. Activating the Molecular Spinterface. *Nat. Mater.* **2017**, *16* (5), 507–515.
- (27) Jiang, X.; Hao, G.; Wang, X.; Mosey, A.; Zhang, X.; Yu, L.; Yost, A. J.; DiChiara, A. D.; N'Diaye, A. T.; Cheng, X.; Zhang, J.; Cheng, R.; Xu, X.; Dowben, P. A. Tunable Spin-State Bistability in a Spin Crossover Molecular Complex. *J. Phys.: Condens. Matter* **2019**, *31* (31), 315401.
- (28) Bousseksou, A.; Molnár, G.; Salmon, L.; Nicolazzi, W. Molecular Spin Crossover Phenomenon: Recent Achievements and Prospects. *Chem. Soc. Rev.* **2011**, 40 (6), 3313–3335.
- (29) Real, J. A.; Gaspar, A. B.; Carmen Muñoz, M. Thermal, Pressure and Light Switchable Spin-Crossover Materials. *Dalton Transactions* **2005**, 2062–2079.

- (30) Bousseksou, A.; Molnár, G.; Demont, P.; Menegotto, J. Observation of a Thermal Hysteresis Loop in the Dielectric Constant of Spin Crossover Complexes: Towards Molecular Memory Devices. *J. Mater. Chem.* **2003**, *13* (9), 2069–2071.
- (31) Ossinger, S.; Näther, C.; Buchholz, A.; Schmidtmann, M.; Mangelsen, S.; Beckhaus, R.; Plass, W.; Tuczek, F. Spin Transition of an Iron(II) Organoborate Complex in Different Polymorphs and in Vacuum-Deposited Thin Films: Influence of Cooperativity. *Inorg. Chem.* **2020**, *59*, 7966–7979.
- (32) Wäckerlin, C.; Donati, F.; Singha, A.; Baltic, R.; Decurtins, S.; Liu, S. X.; Rusponi, S.; Dreiser, J. Excited Spin-State Trapping in Spin Crossover Complexes on Ferroelectric Substrates. *J. Phys. Chem. C* **2018**, *122* (15), 8202–8208.
- (33) Costa, P.; Hao, G.; N'Diaye, A. T.; Routaboul, L.; Braunstein, P.; Zhang, X.; Zhang, J.; Doudin, B.; Enders, A.; Dowben, P. A. Perturbing the Spin Crossover Transition Activation Energies in $Fe(H_2B(Pz)_2)_2(Bipy)$ with Zwitterionic Additions. *J. Phys.: Condens. Matter* **2018**, *30* (30), 305503.
- (34) Carvell, J.; Cheng, R. Study of Electrical Polarization Hysteresis in Ferroelectric Polyvinylidene Fluoride Films. *Mater. Lett.* **2010**, *64* (18), 1992–1995.
- (35) Ducharme, S.; Reece, T. J.; Othon, C. M.; Rannow, R. K. Ferroelectric Polymer Langmuir-Blodgett Films for Nonvolatile Memory Applications. *IEEE Trans. Device Mater. Reliab.* **2005**, *5* (4), 720–735.
- (36) Palamarciuc, T.; Oberg, J. C.; El Hallak, F.; Hirjibehedin, C. F.; Serri, M.; Heutz, S.; Létard, J.-F.; Rosa, P. Spin Crossover Materials Evaporated under Clean High Vacuum and Ultra-High Vacuum Conditions: From Thin Films to Single Molecules. *J. Mater. Chem.* **2012**, 22 (19), 9690.
- (37) He, X.; Yao, K.; Gan, B. K. Phase Transition and Properties of a Ferroelectric Poly(Vinylidene Fluoride-Hexafluoropropylene) Copolymer. *J. Appl. Phys.* **2005**, *97* (8), 084101.
- (38) Bousseksou, A.; Molnár, G. The Spin-Crossover Phenomenon: Towards Molecular Memories. C. R. Chim. **2003**, 6 (8–10), 1175–1183
- (39) Linares, J.; Nasser, J.; Boukheddaden, K.; Bousseksou, A.; Varret, F. Monte Carlo Simulations of Spin-Crossover Transitions Using the Two-Level Model. I: Mononuclear Single Sublattice Case. *J. Magn. Magn. Mater.* **1995**, *140*–*144*, 1507–1508.
- (40) Chiruta, D.; Linares, J.; Dimian, M.; Alayli, Y.; Garcia, Y. Role of Edge Atoms in the Hysteretic Behaviour of 3D Spin Crossover Nanoparticles Revealed by an Ising-like Model. *Eur. J. Inorg. Chem.* **2013**, *2013*, 5086–5093.
- (41) Tagantsev, A. K.; Stolichnov, I.; Colla, E. L.; Setter, N. Polarization Fatigue in Ferroelectric Films: Basic Experimental Findings, Phenomenological Scenarios, and Microscopic Features. *J. Appl. Phys.* **2001**, *90* (3), 1387–1402.
- (42) Gomes, J.; Nunes, J. S.; Sencadas, V.; Lanceros-Mendez, S. Influence of the β -Phase Content and Degree of Crystallinity on the Piezo-and Ferroelectric Properties of Poly(Vinylidene Fluoride). *Smart Mater. Struct.* **2010**, *19* (6), 065010.
- (43) Lefter, C.; Davesne, V.; Salmon, L.; Molnár, G.; Demont, P.; Rotaru, A.; Bousseksou, A. Charge Transport and Electrical Properties of Spin Crossover Materials: Towards Nanoelectronic and Spintronic Devices. *Magnetochemistry* **2016**, 2 (1), 18.
- (44) Mahfoud, T.; Molnár, G.; Cobo, S.; Salmon, L.; Thibault, C.; Vieu, C.; Demont, P.; Bousseksou, A. Electrical Properties and Non-Volatile Memory Effect of the [Fe(HB(Pz)3)2] Spin Crossover Complex Integrated in a Microelectrode Device. *Appl. Phys. Lett.* **2011**, *99* (5), 053307.
- (45) Baadji, N.; Sanvito, S. Giant Resistance Change across the Phase Transition in Spin-Crossover Molecules. *Phys. Rev. Lett.* **2012**, 108 (21), 1–5.
- (46) Rotaru, A.; Gural'Skiy, I. A.; Molnár, G.; Salmon, L.; Demont, P.; Bousseksou, A. Spin State Dependence of Electrical Conductivity of Spin Crossover Materials. *Chem. Commun.* **2012**, *48* (35), 4163–4165.

- (47) Li, F.; Huang, J.; Hu, Y.; Li, Q. Transport Property of Ligand-Driven Light-Induced Spin-Change Fe-Based Spin Crossover Complexes. RSC Adv. 2019, 9 (22), 12339—12345.
- (48) Faulmann, C.; Jacob, K.; Dorbes, S.; Lampert, S.; Malfant, I.; Doublet, M.-L.; Valade, L.; Real, J. A. Electrical Conductivity and Spin Crossover: A New Achievement with a Metal Bis Dithiolene Complex. *Inorg. Chem.* **2007**, *46* (21), 8548–8559.
- (49) Schleicher, F.; Studniarek, M.; Kumar, K. S.; Urbain, E.; Katcko, K.; Chen, J.; Frauhammer, T.; Hervé, M.; Halisdemir, U.; Kandpal, L. M.; Lacour, D.; Riminucci, A.; Joly, L.; Scheurer, F.; Gobaut, B.; Choueikani, F.; Otero, E.; Ohresser, P.; Arabski, J.; Schmerber, G.; Wulfhekel, W.; Beaurepaire, E.; Weber, W.; Boukari, S.; Ruben, M.; Bowen, M. Linking Electronic Transport through a Spin Crossover Thin Film to the Molecular Spin State Using X-Ray Absorption Spectroscopy Operando Techniques. ACS Appl. Mater. Interfaces 2018, 10 (37), 31580–31585.
- (50) Osorio, E. A.; Moth-Poulsen, K.; van der Zant, H. S. J.; Paaske, J.; Hedegård, P.; Flensberg, K.; Bendix, J.; Bjørnholm, T. Electrical Manipulation of Spin States in a Single Electrostatically Gated Transition-Metal Complex. *Nano Lett.* **2010**, *10* (1), 105–110.
- (51) Gopakumar, T. G.; Matino, F.; Naggert, H.; Bannwarth, A.; Tuczek, F.; Berndt, R. Electron-Induced Spin Crossover of Single Molecules in a Bilayer on Gold. *Angew. Chem., Int. Ed.* **2012**, *51* (25), 6262–6266.
- (52) Ruiz, E. Charge Transport Properties of Spin Crossover Systems. *Phys. Chem. Chem. Phys.* **2014**, *16* (1), 14–22.
- (53) Rotaru, A.; Dugay, J.; Tan, R. P.; Guralskiy, I. A.; Salmon, L.; Demont, P.; Carrey, J.; Molnár, G.; Respaud, M.; Bousseksou, A. Nano-Electromanipulation of Spin Crossover Nanorods: Towards Switchable Nanoelectronic Devices. *Adv. Mater.* **2013**, 25 (12), 1745–1749.
- (54) Miyamachi, T.; Gruber, M.; Davesne, V.; Bowen, M.; Boukari, S.; Joly, L.; Scheurer, F.; Rogez, G.; Yamada, T. K.; Ohresser, P.; Beaurepaire, E.; Wulfhekel, W. Robust Spin Crossover and Memristance across a Single Molecule. *Nat. Commun.* **2012**, 3 (1), 938.
- (55) Geest, E. K.; Shakouri, K.; Fu, W. Y.; Robert, V.; Tudor, V.; Bonnet, S.; Schneider, G. F. Contactless Spin Switch Sensing by Chemo-Electric Gating of Graphene. *Adv. Mater.* **2020**, *32*, 1903575.



Addition/Correction pubs.acs.org/JPCL

Correction to "Quantitative Study of the Energy Changes in Voltage-Controlled Spin Crossover Molecular Thin Films"

Aaron Mosey, Ashley S. Dale, Guanhua Hao, Alpha N'Diaye, Peter A. Dowben, and Ruihua Cheng* J. Phys. Chem. Lett. 2020, 11, 19, 8231–8237. DOI: 10.1021/acs.jpclett.0c02209



Cite This: J. Phys. Chem. Lett. 2021, 12, 2463-2463



ACCESS

III Metrics & More

Article Recommendations

n our recent publication, Figure 5 was published without adequate due diligence. The correct TOC Abstract graphic and Figure 5 are contained here in this correction. The correct on to off current ratios are in the range of 4 to 5, not 100 and the signal to noise ratios are far less than previously shown.

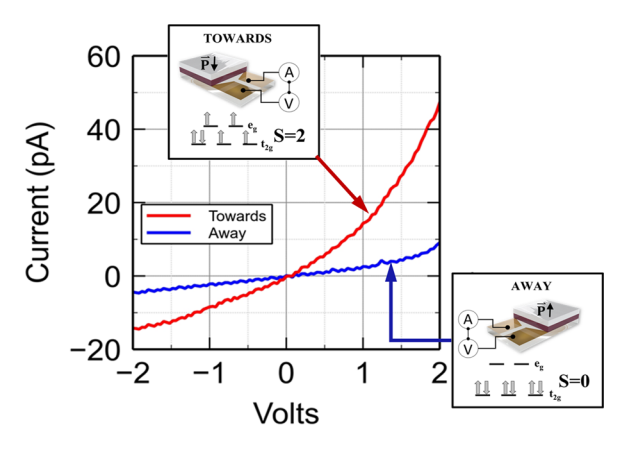
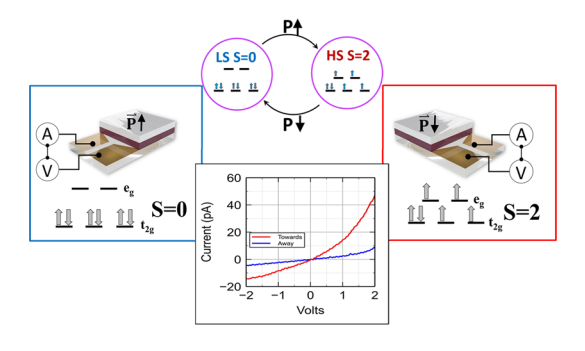


Figure 5. Change in conductance observed with different ferroelectric polarization directions. Transport measurements were taken across a device with the ferroelectric layer adjacent to the SCO layer. Polarizing the ferroelectric toward the $[Fe\{H_2B(pz)_2\}_2(bipy)]$ layer results in HS S = 2, and a larger conductance. Polarization of the ferroelectric away from the $[Fe\{H_2B(pz)_2\}_2(bipy)]$ layer gives the LS S = 0 state and lower conductance. Device type 3 is schematically illustrated.



Published: March 4, 2021



